

# Influencing the Deployment Geometry of Kirigami Lattices Using Integrated Piezoelectric Actuators

Max Vergé-Kemp

School of Civil, Aerospace and Design Engineering, University of Bristol, Queen's Building, University Walk, Bristol. BS8 1TR, UK.

Supervised by

Rainer Groh

## Abstract

The ability to influence the deployment of conventional linear parallel kirigami lattices through the use of piezo-electric actuators permits the creation of deployable structures with in-situ variable tensile stiffness. These lattices exhibit multi-stability when buckling under tensile load: the ability to deform into two possible stability states, one stiffer and the other more flexible in tension. This paper aims to explore the feasibility of integrating piezo elements onto mylar kirigami sheets in order to observe a change in load necessary to deflect them in tension perpendicularly from their cut geometry. In addition to this, numerical models of the kirigami lattices are developed and compared to digital image correlation data to assess their practicality when predicting the deflection characteristic of their experimental counterparts. Initial results show that these computational methods agree with experimental data, falling mostly within a precision range of 3.9-4.8 %, both when predicting deflection geometry and buckling point of cells. Through analysing the load response to tensile deflection of higher stiffness kirigami, a phenomenon of cells popping into a lower energy more flexible state is also observed. The integration of piezo-electrics onto kirigami lattices shows promising results: when arranged horizontally, the actuators allow for a maximum tensile load difference between their powered state and unpowered state of 0.28 N or 11.7 %. For the vertical placement of the piezos, a larger maximum load difference of 0.72 N or 23.2 % occurs between their powered and unpowered state. Further numerical models assess the ability of the simulations to predict the influence of integrated piezos on the kirigami's deflection. Results suggest that although the numerical models adequately compute the deflection characteristic of kirigami with horizontally integrated piezos, they are limited when calculating the response of the kirigami with vertically integrated piezos, as they do not simulate cells popping from a stiffer state to a lower energy flexible state. Positive results show that further efforts in integrating piezo-electrics onto kirigami sheets, coupled with higher performing actuators, would yield the ability to create deployable structures with fully tunable characteristics.

**Key Words:** Kirigami, Multi-stable, Piezo-actuated, Deployable structures, Numerical simulation

## 1 Introduction

Kirigami, the art of folding cut paper, allows for intricate three-dimensional geometries to appear from planar sheets of material. When a load is applied to these lattices, their cells deform into complex shapes with unique behaviours and characteristics [3, 4, 7, 18, 22]. Although most lattices only deform into a single shape, conventional linear parallel kirigami (with all cuts parallel to each other, and perpendicular to the applied load) displays the ability to be nudged between two stability states, one stiffer and the other more flexible, through the use of external forces. As such, could the deployment geometry of these matrices be controlled through the use of integrated actuators, allowing for tuneable structures?

Much like origami, which sees many applications thanks to its ability to pack down and redeploy complex structures [3, 16, 20, 23], kirigami has become a growing subject for research. Highly versatile, this ancient paper cutting art sees many kinds of applications. On one hand, its ability to transform planar sheets of material into three-dimensional structures has been used to engineer self-folding machines [8, 9] deployable honey-comb structures [17], and foldable electronics [25, 29]. Additionally, the response of kirigami to load, presenting itself as the out-of-plane deformation of its cells, allows for

the conception of intricate deployable structures, including soft body crawlers [19], soft grippers [27], local drug delivery systems [2] and low-complexity solar tracking arrays [13].



Figure 1: Deployment geometry of conventional linear parallel multi-stable kirigami lattices [26]: a) symmetric, b) multi-stable, c) anti-symmetric

However, the kirigami matrices developed for these applications are bound to the unique deployment geometry they have been designed for. The recent emergence of a conventional linear parallel multi-stable kirigami [26, 28] however, could offer the means to create structures with variable deployable geometry. Depending on the spacing between their cuts, these lattices can deform into two different stability states, each exhibiting unique characteristics: higher flexibility for the anti-symmetric state shown in Figure 1.c, and higher stiffness for the symmetric state shown in Figure 1.a [26]. If the spacing between these lattices' cuts fall within a certain range however, the kirigami becomes multi-stable, with its cells

being able to deform in either of each stability state, as shown in Figure 1.b. As the cells of these lattices can be nudged [6] into a chosen states when influenced by an external force, it has been shown that the stiffness of the sheets can be tuned in-situ [26], by varying the number of cells deflected in each state. It is further hypothesises in this paper that the deployment geometry of multi-stable kirigami sheets could be controlled with the use of integrated actuators, applying a strain or deformation preload to certain cells, thus influencing their deployment into either a symmetric or anti-symmetric state.

The ability to remotely control the state of selected cells in kirigami matrices would allow for the creation of user-controlled variable stiffness structures. This could see applications for damping out vibrations in systems where load frequencies and rate vary. For example, the ability to vary the stiffness of deployable booms in space applications could help reduce vibrations at their extremities during burns or other manoeuvres.

Control over kirigami lattices' deployment is achieved by preloading certain cells with an applied strain. Piezoelectric actuators are chosen for this in this paper, as they are flexible, provide a localised strain, deform instantaneously when a voltage is applied, and readily available.

In this paper, the study of the multi-stable matrices is performed both experimentally and numerically, to explore the practicality of computational methods for kirigami development. As the use of numerical methods is relatively novel in this field, and has primarily been used to aid in the development of kirigami lattices [1], the models created in this paper serve to establish the accuracy of the tools, and create well-founded techniques for studying kirigami computationally. In order to quantitatively establish the precision of these numerical models, the deformation and strain results produced by the simulations are compared to Digital Image Correlation (DIC) data collected from experimental runs of the same kirigami lattices.

The use of DIC to capture the deflection and strain across a kirigami lattice during its deflection has not been widely explored. While work has been produced analysing strain fields on kirigami to aid in their development [10], the idea of linking experimental values to numerically computed results in order to validate numerical models remains novel. The ability to quantitatively define the displacement and state of kirigami cells, especially in multi-stable lattices, greatly aids in their analysis, and allows for the concrete verification of the computational models.

This report is segmented into two parts. Firstly, tensile experiments are run on a set of three 'comparative' kirigami lattices, whose deflection geometry is known. The data collected from these runs is compared to numerical twins of these lattices, as a means to assess the accuracy of the computational simulation. Secondly, once the model is well defined, tensile tests are run on kirigami lattices hosting integrated actuators, to observe their effect on the kirigami cells' deformation. As previous work [15] has outlined the difficulty of capturing con-

clusive results from similar experiments, due to a large number of unwanted influences linked with the integration of the actuators, these tests are repeated numerically to isolate the impact of the actuators, and obtain more definite results.

## 2 Kirigami Lattice Specifications

Throughout this paper, Cartesian XYZ coordinates are aligned with each kirigami sheet's width wise, span wise and out of plane direction respectively, with an origin set at their lower-left corner, as depicted in Figure 2.

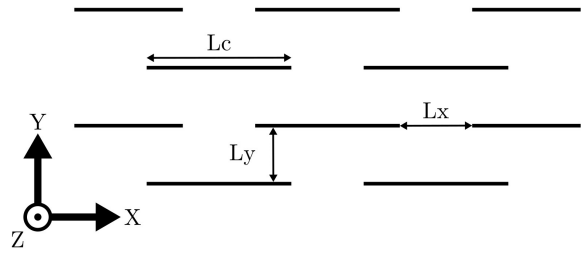


Figure 2: Kirigami sheet coordinate system and parameters

All lattices are defined by  $L_c$ ,  $L_x$  and  $L_y$  values, representing the cut length, horizontal and vertical spacing between cuts respectively, as seen in Figure 2. This research also references  $L_c/L_x$  and  $L_c/L_y$  values as they best describe the behaviour of these kirigami matrices under load [26].

## 3 Experimental Method

### 3.1 Boundary Conditions

As the deployment geometry of kirigami lattices is highly influenced both by defects in the material and by small variations in their loading conditions, particular attention has to be brought to applying adequate boundary conditions during testing. To observe the expected deformation from each matrix, a uniform and uni-directional load must be applied. Furthermore, with the specimens being loaded in tension along their Y-axis, all other degrees of freedom must be restrained on the sheets' lower and upper edges.

To achieve this, 3D-printed clamps serve as a rigid interface between the kirigami sheets and the tensile machine. The clamps' ridged geometry and distributed through-bolts both ensure the load is uniform along the clamped edge, and restricts the displacement and rotation of the sheets [15], especially along their Y-axis, where they are the most prone to slipping when under load.

### 3.2 Materials and Manufacture

The manufacture of the sheets is enabled by both a CNC knife cutter and CNC laser cutter. Due to poorer precision and unsatisfactory cut finish, the use of the CNC knife cutter was quickly abandoned. CNC machines allows for very accurate and consistent slits to be cut into the sheets, ensuring the expected deflection to occur when they are loaded.

Lattice patterns are generated through a MATLAB [11] code, with inputs for Lc, Lc/Lx and Lc/Ly, outputting a file readable by the CNC machines. The script guarantees each cut matrix is centred on the sheets, and that the cut lengths and spacing is uniform and correct.

For this research, kirigami lattices are cut into paper, polypropylene and mylar to assess each material's response. The material who's cells deflect the most consistently guarantees the best experimental results, and thus is the most appropriate to use.

Typical printer paper cuts well on the CNC laser cutter, allowing for a very precise matrix. Promising results arose from a multi-stable matrix, for which a large number of both symmetrically and anti-symmetrically deflected cells appear across the specimens, as shown in Appendix A Figure 18. However, loaded sheets do not return to their initial conditions, as they deform plastically as cells crease, resulting in the sheet being unusable for more than one load cycle. Paper remains an effective material to quickly observe the response of cut matrices to tensile loading.

The kirigami lattices cut into polypropylene sheet are less accurate, as the material melts slightly around the cuts. Despite this, the sheets deflect suitably, and once unloaded return to their initial state. However, only thin sheets of the material could be sourced. As such, lattices have a tendency to rip when handled or loaded excessively. This also leads to the sheets sagging when setup in the tensile machine, even when a preload is applied, skewing obtained results.

Mylar sheets have been used in previous works [15], and are known to host kirigami cut matrices well. The high yield strength of the material allows it to deflect significantly without any permanent deformation appearing. Three thicknesses of mylar are assessed, 0.125 mm, 0.073 mm and 0.023 mm. Much like with polypropylene, the thinner sheets sag when setup in the tensile machine, and as such are disregarded. The 0.125 mm mylar remains planar while still deflecting with relatively low tensile force, and is as such deemed most suitable.

Throughout the rest of this paper, kirigami lattices are cut into 0.125 mm thick mylar, with Young's modulus  $E = 5.3 \text{ GPa}$ , Poisson's ratio  $\nu = 0.3$  and density  $\rho = 1.3 \text{ g/cm}^3$  [5].

### 3.3 Kirigami sheet testing

To observe their deformation in a controlled environment, kirigami sheets are clamped and loaded in a Shimadzu Autograph AGS-X 10 kN tensile testing machine, as can be seen in Figure 3. A tensile deflection of 5 mm is applied to each sheet along their Y-axis, at a rate of 2.5 mm/min. Each sheet is subject to 5 load cycles, recording deflection and load.

A set of three comparative sheets is initially produced to observe the deflection of symmetric, multi-stable and anti-symmetric lattices. Each of these sheets have a relatively small cut length Lc of 15 mm, to maximise the number of cells along the sheet, and thus decrease the effects of the free edges [15]. The cut parameters of these

sheets can be found in Table 1. Lc and Lx values are kept constant for each sheet as controlled variables.

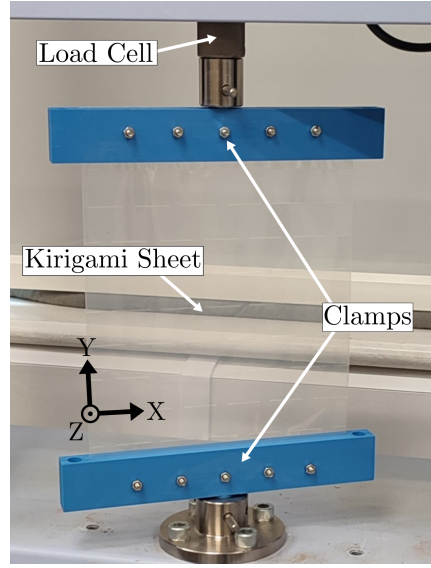


Figure 3: Kirigami tensile test setup

Table 1: Comparative sheets' parameters

Lattice Type	Lc [mm]	Lc/Lx	Lc/Ly
Symmetric	15	3	2
Multi-Stable	15	3	3
Anti-Symmetric	15	3	5

A lower resolution piezo-ready multi-stable (PRMS) sheet, with a cut length Lc of 40 mm, Lx of 13.33 mm and Ly of 16 mm, is manufactured to assess the influence of integrated actuators on the deployment geometry of kirigami lattices. The larger cut length is required for the sheet to accept the smallest available piezo-electric actuators, with a width of 12 mm, between its cuts, both horizontally and vertically, as shown in Figure 4. This sheet is multi-stable, with a slight tendency towards a symmetric deflection of its cells. This is as cells deflected symmetrically are in a higher energy state than cells deflected anti-symmetrically [26], and can more easily be nudged [6] into the opposing state by the actuators. This sheet is loaded both with and without the piezo-electric actuators attached, and with them both powered and unpowered, to assess their influence on the deployment of the sheet. The parameters of this sheet can be found in Table 2

Table 2: PRMS sheet parameters

Lattice Type	Lc [mm]	Lc/Lx	Lc/Ly
Multi-Stable	40	3	2.5

#### 3.3.1 Piezo electric actuators

Piezo-electric actuators are chosen to influence the deployment of the appropriate kirigami sheet. When provided with sufficient voltage, they offer a small out-of-plane bending deflection [15]. These types of actuators have been used to measure the deflection of kirigami lattices, and harness energy from their deformations [12,30], and as such it is hypothesised that when run as actuators they will allow selected cells to pop between states. Due to their relatively small dimensions, with a width of 12 mm, length of 40 mm and thickness of 0.04 mm or 3.15% of the mylar thickness, their implementation onto

the mylar sheets is not expected to significantly influence their deployment unless they are powered.

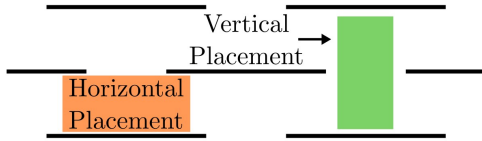


Figure 4: Piezo actuator placements

To actuate the piezo-electrics, a driving circuit used in previous work [15] is selected and improved. A wire harness for the actuators is designed to secure the piezo-electrics' wires to the testing machine while they are integrated onto the kirigami sheets. Furthermore, a desktop power supply is used to power the driving circuit, to accurately control the input voltage, and provide a stable source of current, increasing the reliability of the output voltage to the actuators.

### 3.3.2 Digital Image Correlation

In order to obtain data on the sheets' deflection and strain, DIC (Digital Image Correlation) is adopted. This data can easily be compared to results found through numerical methods, and allows for the development of accurate computational estimates of the deployment geometry of kirigami lattices.

The mylar sheets are readied for DIC analysis by being coated with white aerosol, before a speckled pattern is applied by spraying black aerosol from further above. This creates the random monochrome pattern necessary for DIC to track local displacement and strain throughout the sheet. The added thickness from the paint layers is negligible.

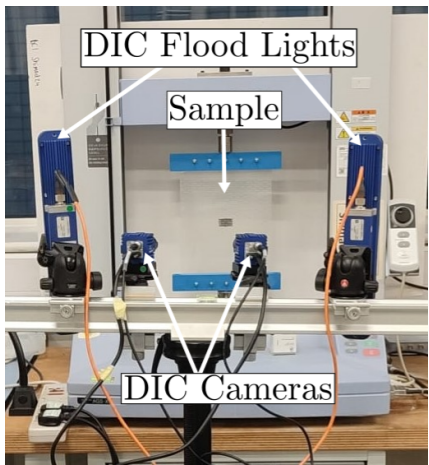


Figure 5: DIC setup

A dual-camera LaVision DIC system is setup as seen in Figure 5. The recording is started in time with the tensile test, at a sample rate of 1.25 Hz, thus capturing a total of 150 pictures per run. Images are processed through the LaVision DaVis software [14], and plotted in MATLAB [11].

## 4 Numerical Method

### 4.1 Kirigami Lattice Model

A numerical twin of each tested lattice was made, allowing for computational analysis of the kirigami within Abaqus [21]. MATLAB [11] was used to define node and quadrilateral stress/displacement shell element placement for each lattice, with inputs of  $L_c$ ,  $L_c/L_x$  and  $L_c/L_y$ , outputting an input file for Abaqus [21]. The meshes outputted contain 190 elements in X, and 305 to 425 elements in Y based on a convergence study, depending on the lattice modelled, each with a zero slit width. Both the upper and lower edges are restricted in all degrees-of-freedom, with the top edge being deflected 5 mm along its Y-axis in tension during the analysis step. A material is created in Abaqus [21] following the properties of the mylar sheets used:  $h = 0.125$  mm,  $E = 5.3$  GPa,  $\nu = 0.3$  and  $\rho = 1.3$  g/cm<sup>3</sup>.

### 4.2 Computational Analyses

The comparative sheets' models are initially computed through a linear buckling analysis, to obtain out-of-plane deflection geometry. As these analyses are fast to compute, they serve mainly as trial beds for each model, to ensure the expected behaviour is computed by the program. For this analysis type, the 5 mm deflection load is ramped linearly over an arbitrary period. To obtain the expected results, positive eigenvalues are requested for each buckling modes, ensuring these are caused by tensile loading.

In order to capture the load history and buckling point of each kirigami, non-linear analyses are run for all models. This analysis type is achieved by running Abaqus' [21] Dynamic Implicit simulations, with the nlgeom (Non-Linear Geometry) setting enabled. These are run with a maximum step size of 1 s, over a period of 120 s, with the 5 mm load linearly ramped over the simulation period, to mirror the experimental method. As this is not a buckling simulation, out-of-plane deformation cannot be observed when running the model, as it remains in a pseudo-stable state. To mitigate this, small perturbations have to be applied in a preloading step. These are modelled as 0.5 mm displacement above and below the three most central slit of a model. With these small loads, all kirigami display the expected out-of-plane deformation geometry.

Non-linear dynamic implicit analyses are chosen when simulating the effect of piezo-electric actuators on the deployment of kirigami lattices. Although quick, linear analyses require more effort to accurately compute the complex deployment resulting from the piezo actuators' influence. The piezo elements are simulated to exert a strain on localised areas of the lattices, both during a 1 s preloading step, and the 120 s analysis steps. Due to the interactions between the piezos and the kirigami, these simulations are run with a maximum time step of 0.2 s, for both the preload and analysis steps.

For both linear and non-linear analyses, surface deflection, reaction forces and strain values are all exported from Abaqus [21] to be compared to collected experimental results.

## 5 Results and Discussion

### 5.1 Comparative sheets

The force required to displace each sheet in tension up to 5 mm is logged, with the median values of all runs plotted in Figure 6. It is apparent that the symmetric sheet requires a larger load to be displaced, with a peak of 30 N at 5 mm. The multi-stable and anti-symmetric sheet both require comparable loads, with peaks of 4 N and 2 N respectively, as the cells of the multi-stable sheet primarily deflected anti-symmetrically when loaded despite not being inclined to do so. This can be explained as the anti-symmetric cell state is a lower energy state [26], and symmetric cell deflections arise due to defect in the material or non-uniform loading. This similarity thus confirms the boundary conditions are correctly applied during the experimental work. As the  $L_c$  and  $L_c/L_x$  values are constant for each sheet, it is inferred that as  $L_c/L_y$  reduces and lattices tend towards more symmetric behaviour, the load necessary to deflect the sheets increases.

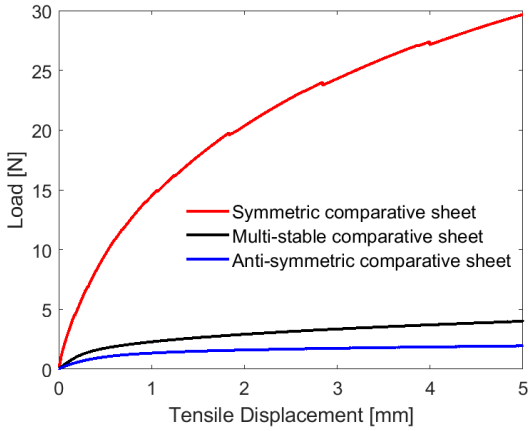
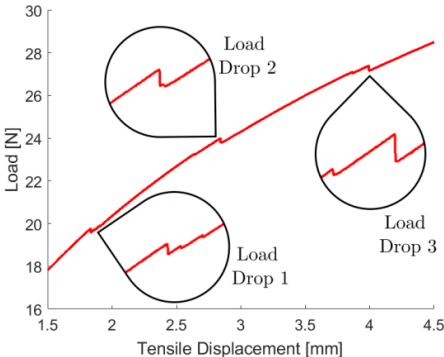
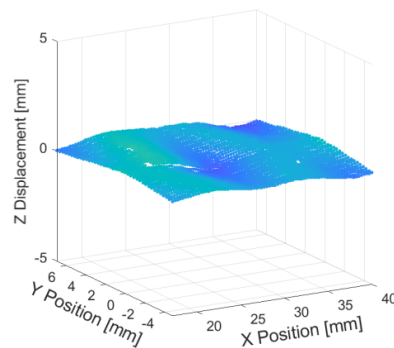


Figure 6: Median load during extension of comparative sheets

Sudden drops in load can be observed when following the deflection history of the symmetric kirigami sheet. The three most distinct cases are outlined in Figure 7.a. This phenomenon is observed to be caused by cells of the sheet popping from a symmetric state into an anti-symmetric state, despite the lattice parameters defining it as fully symmetric.



a) Load drop when extending symmetric comparative sheet



b) DIC Imaging of symmetrically deflected cell, at time t = 45.6 s

As the anti-symmetric state is less stiff than the symmetric state, a small drop in load is observed when this occurs. Figure 7.b and Figure 7.c show a cell switching from a symmetric state to an anti-symmetric state relating to the first load drop in Figure 7.a, captured by the DIC setup. This likely happens as symmetric sheets are bistable, and as the tensile load increases, the bending energy of certain cells surpasses the hinge energy [26] causing them to pop into the anti-symmetric state.

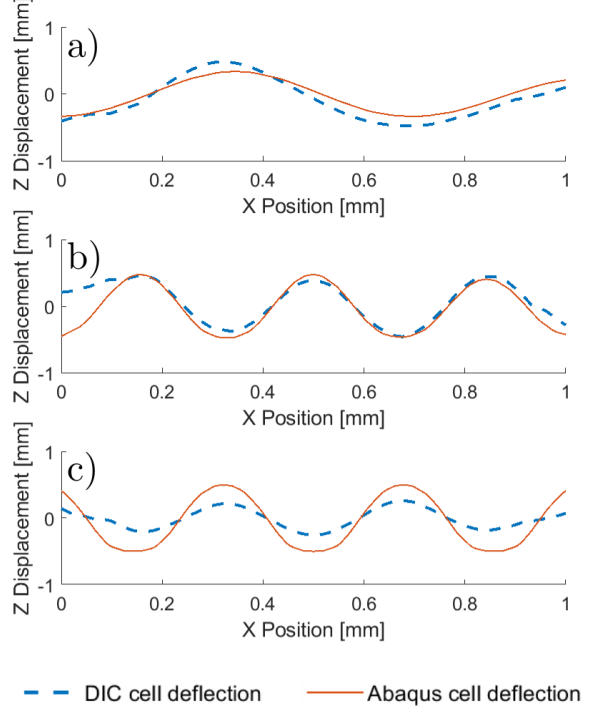
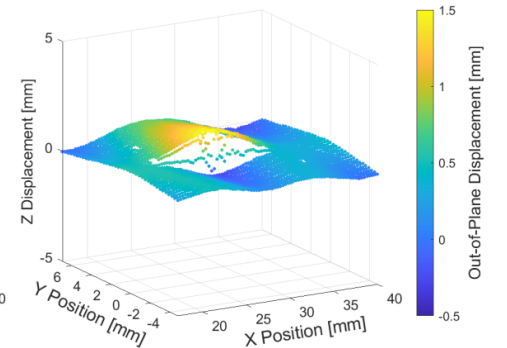


Figure 8: Cut through view of cell deflection of both numerical and experimental comparative sheets: a) Symmetric b) Multi-stable c) Anti-symmetric

Using numerical twins of each kirigami sheet, identical experiments are run in Abaqus [21]. Initially, a linear buckling analysis is run for each lattice to confirm the deflection geometry produced by the software is accurate. Non-linear analyses are then run for the same models, with the results produced being compared to the data collected by the DIC setup, in order to assess the performance and accuracy of the numerical method. Figure 8 presents a cut through view of the out-of-plane de-



b) DIC Imaging of anti-symmetrically deflected cell, at time t = 45.6 s

Figure 7: Cell popping from symmetric to anti-symmetric state when extending symmetric comparative sheet

flection of a set number of cells for both data sets. As the DIC data contains noisy artifacts, the MATLAB [11] *smoothdata* function is used to return cleaner results. The mean difference in deflection for each method is computed and presented in Table 3.

Table 3: Difference in deflection between numerical model and experimental data

Lattice Type	Median Difference	Difference as Percentage of Amplitude
Symmetric	0.117 mm	12.2 %
Multi-Stable	0.0532 mm	5.8 %
Anti-Symmetric	0.233 mm	45.5 %

A relatively large difference in amplitude is observed between actual deflection values and non-linear numerical deflection values. With an error of 45.5 % of the deflection amplitude, the anti-symmetric lattice model is the least accurate. The multi-stable lattice has a lower error value of 5.8 % of the deflection amplitude, suggesting that the larger the deflection amplitude, the more accurate the model becomes. This may be due to the presence of artifacts and noise in the DIC data. As the magnitude of the noise is not proportional to the deflection amplitude of the lattices, it has a more prominent effect for lower amplitude deflection data. If each data sets is normalised to a unit amplitude, the median error drop to 3.9 %, 4.8 % and 4.5 % for the symmetric, multi-stable and anti-symmetric kirigami respectively. These more reasonable values suggest that Abaqus [21] correctly predicts the state each cell will buckle towards for each lattice type, further shown in Appendix B Figures 19, 20, 21. As such, despite the inaccuracy when simulating the deflection amplitude of the kirigami, the model correctly find the general buckling geometry of the cells of each lattice. If precise amplitude values were desired from the numerical model, correction factors could be computed by comparing a larger set of experimental data to their computational counterparts.

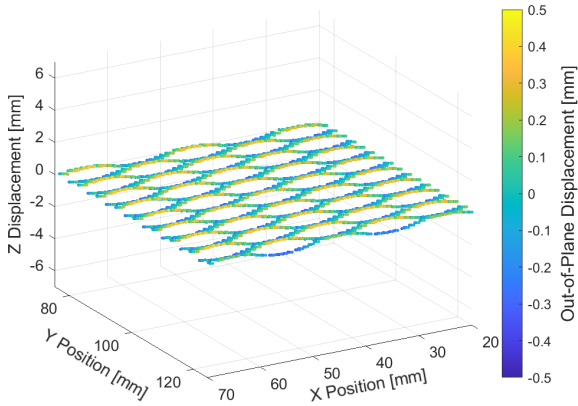


Figure 9: DIC imaging of anti-symmetric sheet deflection at its buckling point

To further explore the practicality of the computation models, the buckling point of each sheet is recorded from the non-linear analyses. In this paper, the buckling point of a lattice is defined as the necessary tensile deflection that must be applied to the sheet to observe an out-of-plane deformation at each cell of at least 0.5 mm, as illustrated in Figure 9. The buckling point of a multi-stable kirigami is a useful parameter to compute, as once cells

have started to deform out-of-plane, they are very unlikely to switch states, unless excessively loaded as seen previously with certain cells of the symmetric sheet popping into an anti-symmetric state. As the stiffness of a lattice can be determined by the state of its cells [26], the buckling point determines the deflection at which the stiffness of the kirigami lattice can confidently be predicted based on its cells behaviour. To assess the numerical model's results, the buckling points of the experimental kirigami sheets are averaged, and compared to their computational counterpart, as presented in Table 4.

Table 4: Numerical and experimental buckling point for comparative sheets

Lattice Type	Median Experimental Buckling Point	Numerical Buckling Points
Symmetric	1.44 mm	1.79 mm
Multi-Stable	1.56 mm	1.62 mm
Anti-Symmetric	1.17 mm	1.22 mm

The variation between the experimental and numerical data is of -24.3 % for the symmetric sheet, -3.9 % for the multi-stable sheet and -4.3 % for the anti-symmetric sheet. As slight tensile preload has to be applied to the experimental kirigami to ensure it is not sagging, inaccuracies may have arisen in the buckling point readings of these experiments. This explains why the computational simulation typically overestimates the buckling point of the kirigami. Unlike with the experimental test, the lattice models start with a true zero deflection, and reach the buckling point later than the preloaded experimental lattices. As Abaqus [21] returns a higher deflection than necessary to reach the buckling point, it can be used to estimate a point of certainty for when the cells of a given kirigami have settled into their stability state.

As the errors between the numerical and experimental data mostly falls under 5 %, it can be said that the computational methods accurately predict both the deflection geometry and buckling point of the comparative kirigami.

## 5.2 Influencing deployment with piezo-actuators

A piezo-ready multi-stable (PRMS) sheet with an inclination towards symmetric deflection is chosen to assess the influence of piezo-actuators on the deflection geometry of kirigami, as defined in Table 2. These lattice parameters are chosen for two primary reasons: Firstly, although symmetric and multi-stable sheets are bistable, anti-symmetric sheets are monostable, and their cells cannot remain deflected symmetrically in a stable manner. Secondly, it has been shown that the cells of well-bounded multi-stable kirigami deflect primarily in an anti-symmetric manner, as this is the lower energy state. Due to this, it is hypothesised that the symmetrically inclined multi-stable sheet will be most prone to the effects of integrated actuators. It is expected that the cells of this sheet deflect anti-symmetrically when no piezo actuators are present, as seen with the previous multi-stable sheet, but with a lower energy input necessary to nudge [6] them to deflect symmetrically.

The piezo elements are situated such that their deformation applies a useful strain to the lattice. Both a vertical and horizontal arrangement of the components is defined, as shown in Figure 10, to assess which is most influential on the deployment behaviour of the kirigami. Vertically, they are applied such that for every row, the deformation of the piezos alternates between positive and negative along the Y axis, further represented by a + and a - respectively in Figure 10. This is done as the vertical area between cuts remains planar when the cells of a lattice deflect anti-symmetrically, and deform alternatively out-of-plane between every row of cuts when the cells deflect symmetrically, further illustrated in Appendix B Figures 22, 23. For the horizontal placement of the piezos, the direction of deflection varies for each column of elements, as shown in Figure 10. This is done as when a lattice deflects symmetrically, the area above and below a cut deflects in the same direction for all cuts in a column, while alternative along a row of cuts. When a lattice deflects anti-symmetrically, this area deflects alternatively both above and below the cut and along a row of cuts, further illustrated in Appendix B Figures 22, 23.

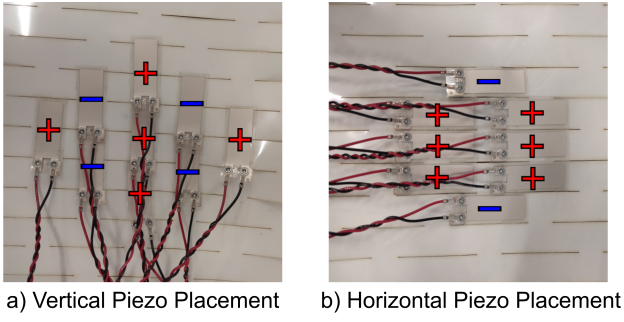


Figure 10: Piezo placement on PRMS kirigami sheet

For both the horizontal and vertical placement of the elements, the piezos are thus arranged such that they influence the lattice to behave more symmetrically, and as such be stiffer, when they are powered, and more anti-symmetric, or flexible, when they are unpowered.

Initial experiments are run comparing the load response of the PRMS sheet both with and without the piezo-actuators. For these initial tests, the piezos are unpowered, to assess how their presence influences the deployment of the kirigami. The load response for the three

cases are presented in Figure 11. It can be seen that while the horizontal placement increases the overall load necessary to deflect the lattice, from requiring 3.83 N to requiring 4.31 N to deflect to 5 mm, the vertical placement reduces it slightly, requiring 3.75 N. This is coherent with the expected behaviour of the kirigami. The added rigidity to the horizontal area between the cuts caused by the piezo integration means a higher load is necessary to deflect these cells, thus increasing the load necessary to deflect the entire lattice. For the vertical arrangement of the piezo elements, the added rigidity in the vertical area between cuts does not increase the load necessary to deflect the kirigami, but rather influences the affected cells to deflect anti-symmetrically at a quicker rate; their buckling point is reduced. This explains why the load necessary to deflect this lattice is initially lower than the datum sheet, but approaches the 3.83 N required to deform the datum sheet as it nears 5 mm of deflection.

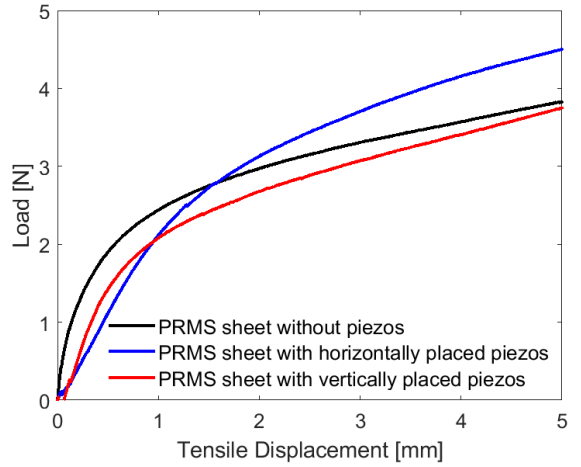


Figure 11: Load necessary to deflect PRMS sheet with and without unpowered integrated piezo elements

The effect on the kirigami's deflection of powering the piezo-actuators is then explored. The elements are supplied with 800 V to obtain noticeable deflection and strain [15], before tensile load is applied to the lattices, with power being sustained throughout the entirety of the kirigami's load cycle.

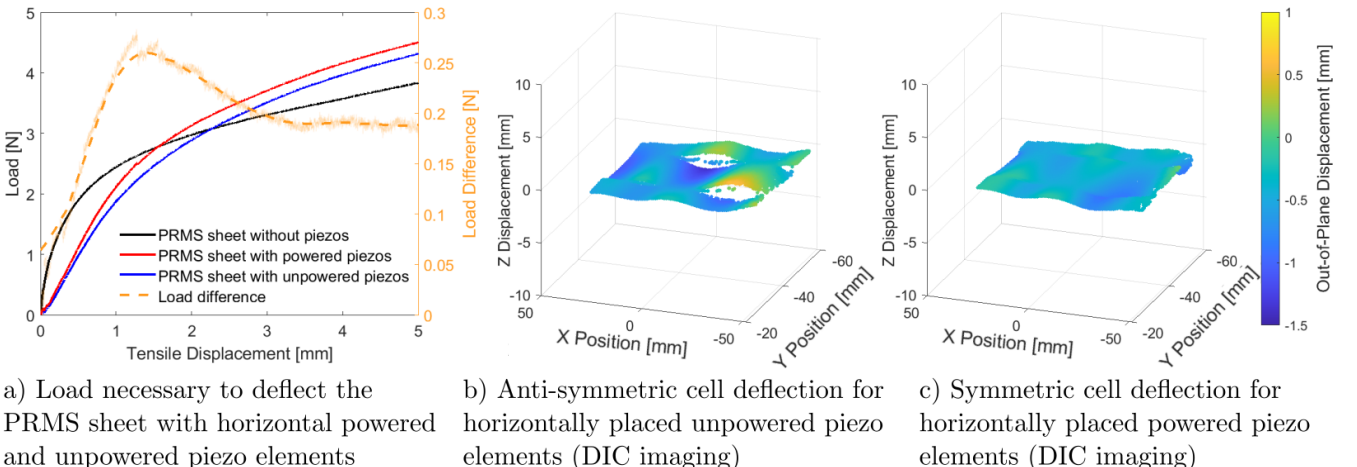


Figure 12: Response of PRMS sheet with horizontally integrated piezo elements

The response of the lattice to the powered horizontally placed piezo-actuators is illustrated in Figure 12.a. As expected, once powered the piezos raise the secant stiffness to 5 mm of the kirigami, as they slightly influence it to deform symmetrically. Figure 12.b and Figure 12.c show the response of a select set of cells to the piezo actuators being powered. It is clear that when the piezos are unpowered, these cells deflect anti-symmetrically, whilst the opposite is true when the piezos are powered. When comparing the load necessary to deflect the lattice with the piezo elements both powered and unpowered, a maximum difference of 0.26 N (11.6 %) is observed at a deflection of 1.41 mm. At 5 mm of deflection, this difference is of 0.19 N. This is equivalent to an increase in load of 0.66 N, or 17.8 %, at 5 mm of deflection when compared to the datum PRMS sheet.

Alternatively, the response of the lattice to the powered vertically placed piezo-actuators is shown in Figure 13. The load necessary to deflect this lattice rises higher than that needed to deflect both the datum sheet and PRMS sheet hosting the vertical unpowered piezos, but suddenly drops both at 4.33 mm and 4.85 mm of deflection. This phenomenon is similar to that observed with the comparative symmetric kirigami, where cells popped into an anti-symmetric state above a certain threshold, lowering the load needed to deflect the sheet. From 1.54 mm to 4.33 mm of deflection, the difference in load between the sheets hosting the powered and unpowered piezos is relatively constant, with a magnitude of 0.72 N (23.2 %). When compared to the datum PRMS sheet, this is equivalent to an average increase in load of 0.5 N, or 14.8 %. No meaningful data could be extracted from the DIC readings for the vertical placement of the piezo elements, as presented in Appendix C Figure 24.

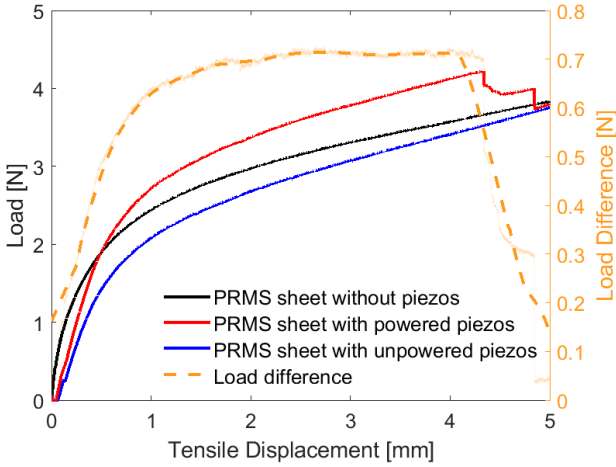


Figure 13: Load necessary to deflect PRMS sheet with vertical powered and unpowered piezo elements

The piezo-electric actuators have a clear impact on the stiffness of the PRMS lattice. While the horizontally placed piezos provide only a slight increase in tensile load necessary to deflect the sheet when powered, the vertically placed elements significantly increase the stiffness of the kirigami. The vertical placement can be deemed more useful as the increase in load necessary to deflect the kirigami it creates is relatively stable across a deflection range of 2.79 mm. However, as the difference collapses past 4.33 mm of deflection, the horizon-

tal placement is more suitable for higher deflection use cases.

It is thus possible to control the deployment geometry of kirigami through the implementation of piezo-electric actuators. Despite this, the actuators do not provide enough strain to influence cells to deflect symmetrically for the entirety of the load cycle. Although certain cells initially deflect symmetrically, as seen in Figure 12.c, these pop into the anti-symmetric state when the tensile deflection of the sheet is increased. The ability to force cells into a symmetric state over a larger tensile displacement would allow for a greater stiffness difference to arise between the powered and unpowered state of a piezo-equipped PRMS sheet.

### 5.3 Simulating the influence of piezo-electric actuators

As shown in previous work [15], many unwanted influences to the kirigami sheets' deployment arise from the integration of piezo-electric actuators, such as their wire's stiffness or weight distorting cells. Although efforts have been made to reduce these drawbacks, they have not been fully eliminated. To isolate the influence of the actuators on the deployment of kirigami, they are simulated numerically, with a dynamic implicit solver. As the computational model has been shown to accurately simulate the behaviour of kirigami, it is deemed as a suitable solution to predict the effects of piezo actuators on their deployment, and as such aid in the development of remotely controlled kirigami lattices.

As shown in Equation 1, the strain produced by a piezo element is a factor of both the applied electric field and piezo-electric coefficient, a material property. Similarly, thermal strain is a product of both temperature and the thermal expansion coefficient of the material, as illustrated in Equation 2. As both strains can be equated to each other through a conversion factor  $k$ , shown in Equation 3, the strain produced by a piezo-electric actuator can be modelled as a thermal strain.

$$\epsilon_p = Ed_{33} \quad (1)$$

$$\epsilon_h = \Delta T \alpha \quad (2)$$

$$\epsilon_p = k\epsilon_h \quad (3)$$

with  $\epsilon_p$  the piezo strain,  $\epsilon_h$  the thermal strain,  $d_{33}$  the piezo-electric coefficient [ $C/N$ ],  $E$  the electric field component [ $V/m$ ],  $\Delta T$  the temperature change [ $K$ ] and  $\alpha$  the coefficient of thermal expansion [ $K^{-1}$ ].

Therefore, the piezo-electric actuators are modelled as a thin sheet with a thermal expansion coefficient of  $1 \cdot 10^{-5} K^{-1}$ . In previous work [15], the piezo elements are seen to deflect up to 0.9 mm out-of-plane when supplied with 800 V, and as such the value for the numerical temperature field is iterated over until the value to deflect the simulated piezo elements to 0.9 mm is found. With a value for  $\Delta T$  of 15 K, the numerical piezo actuator deflects as expected, shown in Figure 14.a. The conversion factor between the numerical temperature field to experimental applied voltage is thus  $k = 53.33$ . The elements are then applied to the kirigami through Abaqus'

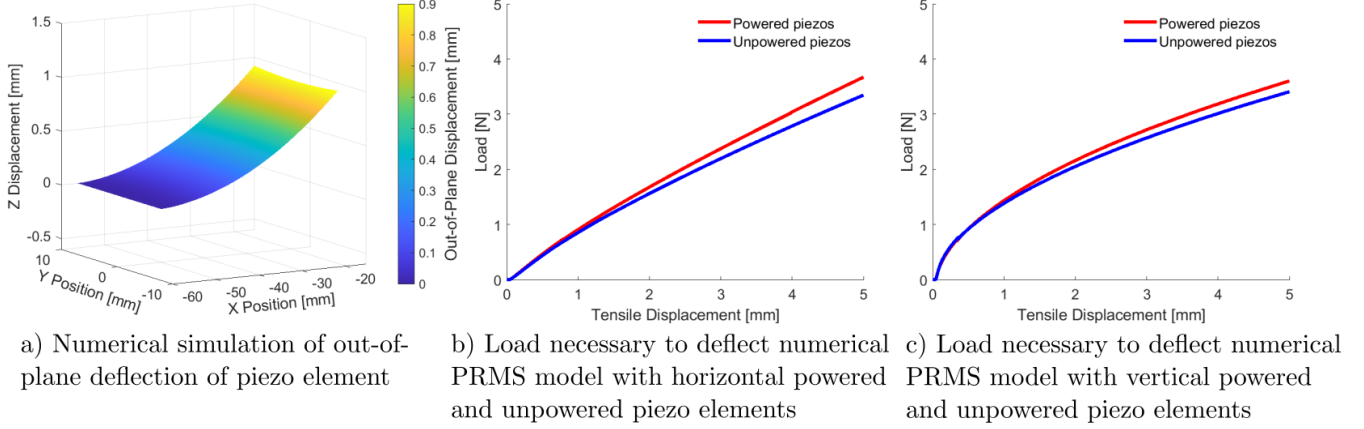


Figure 14: Simulated load response for numerical PRMS model with horizontally and vertically integrated piezo elements

[21] composite layup function, affixing each piezo to the kirigami as presented in Figure 10. To simulate the strain applied to the lattices' cells by powering the piezos both prior to and during their tensile loading, a preload step is integrated into the model, during which a thermal field influences the modelled piezo actuators to deflect. This thermal field continues to be applied throughout the simulation. Both the vertical and horizontal placement of the piezos is simulated, with the load necessary to deflect each kirigami up to 5 mm presented in Figure 14.b and Figure 14.c.

For both the horizontal and vertical placement of the piezo actuators, the maximum tensile load difference between the powered state and unpowered state of the piezos occurs at the maximum tensile deflection of 5 mm. This is different to both experimental cases, during which the maximum load difference occurs between 1.3-1.6 mm of tensile deflection. From the trend of the numerical simulation data, it can be assumed that the maximum tensile load difference will continue to rise as the tensile displacement increases.

For the horizontal placement, the lattice requires 3.37 N of tensile load to deflect up to 5 mm when the piezos are unpowered, and 3.7 N when they are powered. This difference of 0.33 N between both cases, or 9.9 %, is very similar to the maximum experimental difference of 0.28 N, or 11.7 %. For the vertical placement, a tensile load of 3.42 N of tensile load is required to deflect the lattice to 5 mm when the piezos are unpowered, and 3.62 N when powered. This difference in load of 0.2 N, or 5.8 % is 3.6 times lower than the maximum experimental difference of 0.72 N.

When comparing the response of the experimental runs to the simulated results, it can be said that the numerical model of the horizontal piezo placement produces more accurate results than that of the vertical piezo placement. This is due to the fact that the computational model does not predict symmetric cells popping into the anti-symmetric state, a behaviour of these kirigami lattices that result in sudden and drastic tensile load variations. Due to this, the displacement-load history of the simulated kirigami for the vertical piezo placement does not closely match that of the experimental runs.

Further models are run to compute the strain input from the piezo actuators necessary for the affected cells to reach their buckling point during the preloading step of the simulation. It is hypothesised that by influencing cells to reach their buckling point before tensile load is applied, a larger load difference between the powered and unpowered state will occur: as the piezo actuators force cells towards symmetric deflection, they will reach their buckling point and continue to deflect symmetrically throughout the tensile loading of the kirigami.

For the horizontal piezo placement, a thermal field value  $\Delta T$  of 150 K must be applied to obtain a deflection of 0.5 mm at the cells' edges, equivalent to their buckling point. For the vertical piezo placement, the thermal field must be raised to a  $\Delta T$  of 400 K for cells to reach their buckling point. Applying the conversion factor  $k = 53.33$ , this equates to a voltage of 8000 V for the horizontal placement, and 21333 V for the vertical case, higher values that feasible with the piezo driver circuit used in this research.

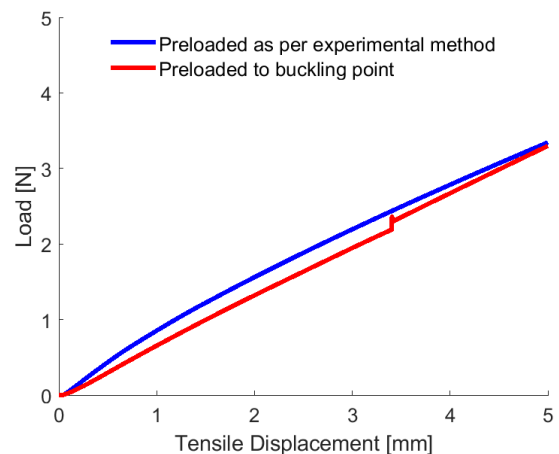


Figure 15: Load necessary to deflect numerical PRMS model with horizontal buckling point preload

Figure 15 illustrate the load necessary to deflect the model of the PRMS sheet when it is preloaded to its buckling point by horizontally placed piezo elements. Unlike hypothesised, the simulation predicts that increasing the preload deformation results in less load being necessary to deflect the kirigami to 5 mm, reducing

the value from 3.7 N with the experimentally accurate preload to 3.28 N, equalling a reduction of -11.4 %. This is due to a majority of the cells being observed to deform anti-symmetrically, reducing the final stiffness of the kirigami. These results suggest that the numerical model is limited when studying the impact of piezo actuators on the deflection of kirigami. The placement of the piezos should lead to the sheet's cells primarily deflecting symmetrically, and causing an increase in load necessary to deflect it in tension. Furthermore, a sudden spike in load for the highly preloaded sheet can be seen at a deflection of 3.48 mm. This phenomenon has not been observed in any experimental runs, which further point towards inaccuracies in the numerical solution.

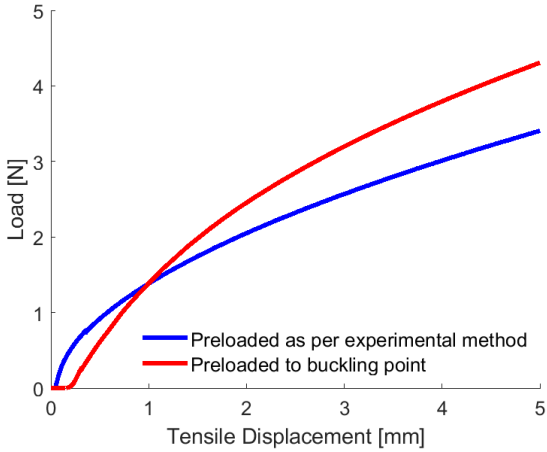


Figure 16: Load necessary to deflect numerical PRMS model with vertical buckling point preload

When the buckling point is reached through the use of vertically placed piezo elements however, a increase in load can be found, as seen in Figure 16. The load necessary to deflect this sheet rises from 3.62 N with the experimental preload, to 4.28 N, or an increase of 18.2 %. This closely relates to expected results, and data found from experimental runs. As the piezo elements force cells to buckle into a symmetric state prior to any tensile loading being applied to the kirigami, these cells continue to deflect towards the higher energy state, resulting in a stiffer deployed structure. Figure 17 confirms a large majority of the lattice's cells deploy symmetrically, even as the kirigami is deflected up to 5 mm. These results suggest that a larger variation in load needed to deflect kirigami could be achieved with more powerful actuators, providing higher localised strain.

#### 5.4 Limitations of DIC

Due to the position of the DIC cameras and the high out-of-plane deflection values observed from the kirigami lattices once loaded, DIC data is occasionally limited. To obtain out-of-plane deflection and strain readings, the pair of DIC cameras must be slightly angled inwards, shown in Figure 5. This limits the area of the kirigami sheet that is in the focal plane of both cameras at once. As DIC data can only be extracted and processed from this compounded area, only a relatively small fraction of the lattices translate into data. This then leads to only a handful of cells being observable from the DIC data, especially with the larger-celled PRMS sheet.

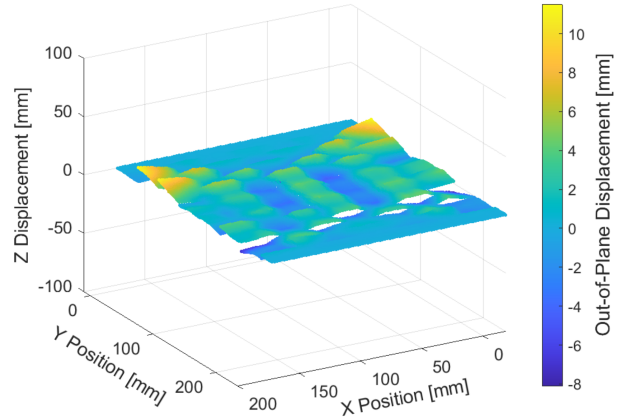


Figure 17: Abaqus model of symmetric deflection of PRMS sheet's cells when preloaded vertically to its buckling point, with 5 mm of tensile deflection

Furthermore, as the cells deflect out-of-plane, certain segments of the lattice previously in focus exit the focal plane, resulting in a loss of data or the apparition of artefacts and noise [24], especially visible in Appendix C Figure 24. This effect is most prominent around the edge of the DIC data, however losses can also be observed throughout the lattices' digital representation. To mitigate this, smoothing functions are applied to the DIC data where necessary, reducing the impact of noise and data loss.

Lastly, DIC analysis's post-processing step assumes the surface observed by the DIC cameras is continuous. As kirigami surfaces contain a large number of slits, and discontinuities in the surface appear once they are deflected, the post-processing step creates unwanted data between the edges of each slit, through interpolation, resulting in additional workload being required to process data into clear figures and results.

## 6 Conclusion

This paper studied the integration of piezo-electric actuators onto kirigami lattices as a means to affect their deployment. Results show that for both configurations considered, an increase in reaction force when loading the kirigami in tension is observed if the integrated piezo elements are powered on. With a vertical configuration, a consistent load difference of 0.72 N (23.2%) can be observed for lower deflection values ranging from approximately 1 mm to 4.5 mm. For the horizontal configuration, the difference in load stabilises for higher deflections at a value of 0.19 N.

Methods for utilising DIC and numerical simulations with kirigami studies are also treated in this research. Although occasionally limited, DIC data treatment proved critical when confirming the behaviour of individual cells of the lattices, and explaining the load response of different cut patterns or piezo configuration. The digitization of the kirigami's out-of-plane displacement and strain when loaded allowed for the development and verification of computational methods for simulation kirigami. Experimental data could easily be compared to results collected from numerical twins of each

lattice, allowing for measurable differences to be computed between both methods.

Although the computational model proved to be accurate when simulating the behaviour of comparative kirigami sheets, it remains limited when implementing piezo actuators. This is especially true when it is presented with extreme piezo deflection values, for which the model's accuracy and results must be questioned.

If future work is to be led following this research, it is suggested to pursue a vertical arrangement of piezo-electric elements in order to observe larger differences in the load needed to deflect the kirigami lattices. Furthermore, a fully symmetric sheet should be adopted as the base for integrating piezo actuators, as cells have a large tendency to deform anti-symmetrically when using a multi-stable sheet. It is expected that a larger range of control should be achieved by sourcing more efficient actuators, and providing higher strain to the cells during preload.

## References

- [1] Nicolas A Alderete, Nibir Pathak, and Horacio D Espinosa. Machine learning assisted design of shape-programmable 3d kirigami metamaterials. *npj Computational Materials*, 8(1):191, 2022.
- [2] Sahab Babaee, Yichao Shi, Saeed Abbasalizadeh, Siddartha Tamang, Kaitlyn Hess, Joy E Collins, Keiko Ishida, Aaron Lopes, Michael Williams, Mazen Albaghddadi, et al. Kirigami-inspired stents for sustained local delivery of therapeutics. *Nature Materials*, 20(8):1085–1092, 2021.
- [3] Sebastien JP Callens and Amir A Zadpoor. From flat sheets to curved geometries: Origami and kirigami approaches. *Materials Today*, 21(3):241–264, 2018.
- [4] Gary PT Choi, Levi H Dudte, and L Mahadevan. Compact reconfigurable kirigami. *Physical Review Research*, 3(4):043030, 2021.
- [5] RS Components. Mylar plastic film, 304mm x 200mm x 0.125mm | rs. <https://uk.rs-online.com/web/p/plastic-film/7850798?gb=s>.
- [6] BS Cox, RMJ Groh, Daniele Avitabile, and A Pirrera. Modal nudging in nonlinear elasticity: Tailoring the elastic post-buckling behaviour of engineering structures. *Journal of the Mechanics and Physics of Solids*, 116:135–149, 2018.
- [7] Marcelo A Dias, Michael P McCarron, Daniel Rayneau-Kirkhope, Paul Z Hanakata, David K Campbell, Harold S Park, and Douglas P Holmes. Kirigami actuators. *Soft matter*, 13(48):9087–9092, 2017.
- [8] Samuel Felton, Michael Tolley, Erik Demaine, Daniela Rus, and Robert Wood. A method for building self-folding machines. *Science*, 345(6197):644–646, 2014.
- [9] Samuel M. Felton, Michael T. Tolley, ByungHyun Shin, Cagdas D. Onal, Erik D. Demaine, Daniela Rus, and Robert J. Wood. Self-folding with shape memory composites. *Soft Matter*, 9:7688–7694, 2013.
- [10] ABM Tahidul Haque, Dohgyu Hwang, and Michael D Bartlett. Graded kirigami composites for programmed strain distributions. *Advanced Materials Technologies*, 7(7):210241, 2022.
- [11] The MathWorks Inc. Matlab 24.2.0.2806996 (r2024b) update 3. <https://www.mathworks.com>, 2024.
- [12] Young-Gyun Kim, Ji-Hyeon Song, Seongheon Hong, and Sung-Hoon Ahn. Piezoelectric strain sensor with high sensitivity and high stretchability based on kirigami design cutting. *npj Flexible Electronics*, 6(1):52, 2022.
- [13] Aaron Lamoureux, Kyusang Lee, Matthew Shlian, Stephen R Forrest, and Max Shteyn. Dynamic kirigami structures for integrated solar tracking. *Nature communications*, 6(1):8092, 2015.
- [14] LaVision. Davis 10. <https://www.lavision.de/en/products/davis-software/index.php>, 2020.
- [15] Vergé-Kemp Max. Integrating piezoelectric actuators onto kirigami matrices to influence their deployment. *University of Bristol RP3*, 2024.
- [16] Marco Meloni, Jianguo Cai, Qian Zhang, Daniel Sang-Hoon Lee, Meng Li, Ruijun Ma, Teo Emilov Parashkevov, and Jian Feng. Engineering origami: A comprehensive review of recent applications, design methods, and tools. *Advanced Science*, 8(13):2000636, 2021.
- [17] Robin M Neville, Jianguo Chen, Xiaogang Guo, Fenghua Zhang, Wenxin Wang, Yousef Dobah, Fabrizio Scarpa, Jin-song Leng, and Hua-Xin Peng. A kirigami shape memory polymer honeycomb concept for deployment. *Smart Materials and Structures*, 26(5):05LT03, 2017.
- [18] Ahmad Rafsanjani and Katia Bertoldi. Buckling-induced kirigami. *Physical review letters*, 118(8):084301, 2017.
- [19] Ahmad Rafsanjani, Yuerou Zhang, Bangyuan Liu, Shmuel M Rubinstein, and Katia Bertoldi. Kirigami skins make a simple soft actuator crawl. *Science Robotics*, 3(15):eaar7555, 2018.
- [20] Syed Imran Hussain Shah, Shahid Bashir, Mubashir Ashfaq, Ahsan Altaf, and Hatem Rmili. Lightweight and low-cost deployable origami antennas—a review. *IEEE Access*, 9:86429–86448, 2021.
- [21] Michael Smith. *ABAQUS/Standard User's Manual, Version 6.9*. Dassault Systèmes Simulia Corp, United States, 2009.
- [22] Jiayue Tao, Hesameddin Khosravi, Vishrut Deshpande, and Suyi Li. Engineering by cuts: how kirigami principle enables unique mechanical properties and functionalities. *Advanced Science*, 10(1):2204733, 2023.
- [23] Nicholas Turner, Bill Goodwine, and Mihir Sen. A review of origami applications in mechanical engineering. *Proceedings of the Institution of Mechanical Engineers, Part C: Journal of Mechanical Engineering Science*, 230(14):2345–2362, 2016.
- [24] Lu Wang, Guangyan Liu, Yawen Deng, Wenzhang Sun, Qinwei Ma, and Shaopeng Ma. Investigation on out-of-plane displacement measurements of thin films via a mechanical constraint-based 3d-dic technique. *Optics Communications*, 530:129015, 2023.
- [25] Tilo H Yang, Hikaru Hida, Daiki Ichige, Jun Mizuno, C Robert Kao, and Jun Shintake. Foldable kirigami paper electronics. *physica status solidi (a)*, 217(9):1900891, 2020.
- [26] Yi Yang, Marcelo A Dias, and Douglas P Holmes. Multistable kirigami for tunable architected materials. *Physical Review Materials*, 2:110601, 11 2018.
- [27] Yi Yang, Katherine Vella, and Douglas P Holmes. Grasping with kirigami shells. *Science Robotics*, 6(54):eabd6426, 2021.
- [28] Yang Yu, Yanqi Yin, Ruiyu Bai, Yunzhou Hu, Bo Li, Michael Yu Wang, and Guimin Chen. Reprogrammable multistable ribbon kirigami with a wide cut. *Applied Physics Letters*, 123(1), 2023.
- [29] Zhuolei Zhang, Yun Yu, Yichao Tang, Ying-shi Guan, Yong Hu, Jie Yin, Katherine Willets, and Shenqiang Ren. Kirigami-inspired stretchable conjugated electronics. *Advanced Electronic Materials*, 6(1):1900929, 2020.
- [30] Xinran Zhou, Kaushik Parida, Oded Halevi, Yizhi Liu, Jiaqing Xiong, Shlomo Magdassi, and Pooi See Lee. All 3d-printed stretchable piezoelectric nanogenerator with non-protruding kirigami structure. *Nano Energy*, 72:104676, 2020.

## 7 Appendices

### Appendix A: Paper kirigami

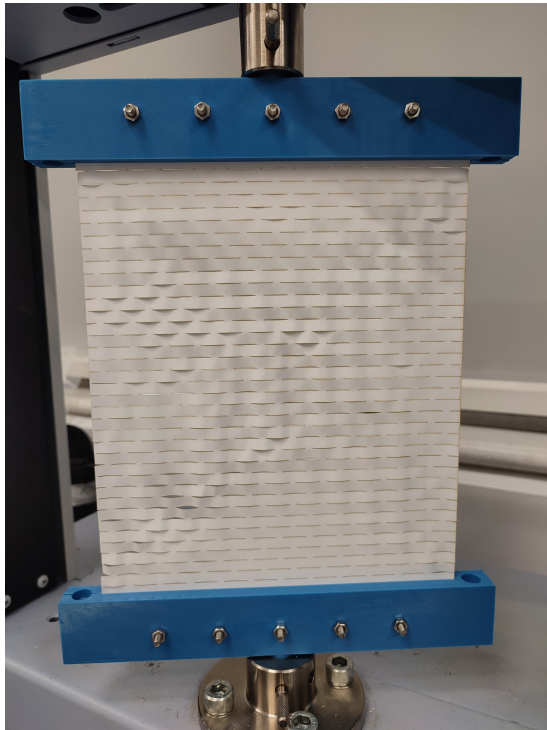


Figure 18: Multi-stable deflection of paper kirigami

### Appendix B: Abaqus models of kirigami deflection states

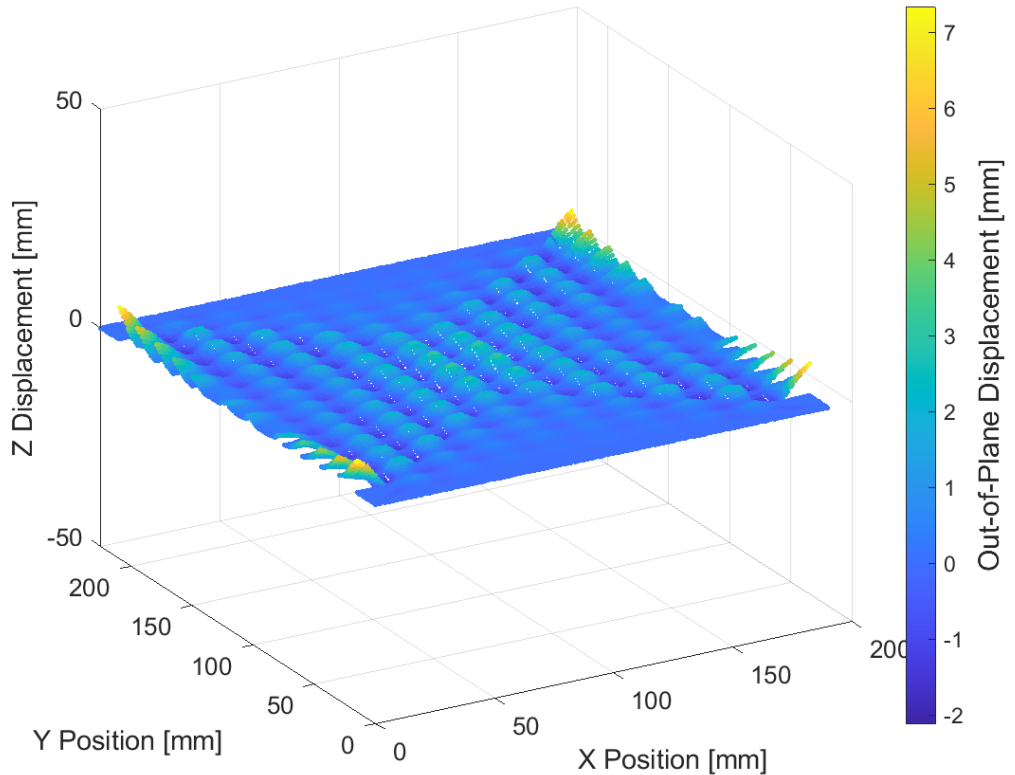


Figure 19: Symmetric lattice deflection

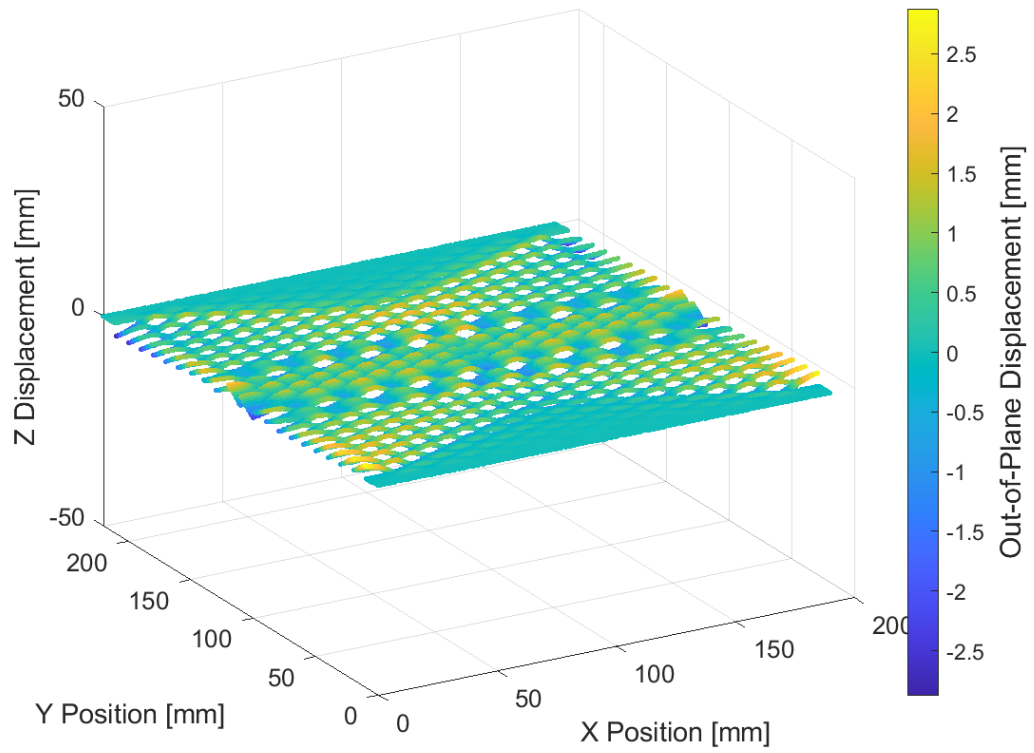


Figure 20: Multi-stable lattice deflection

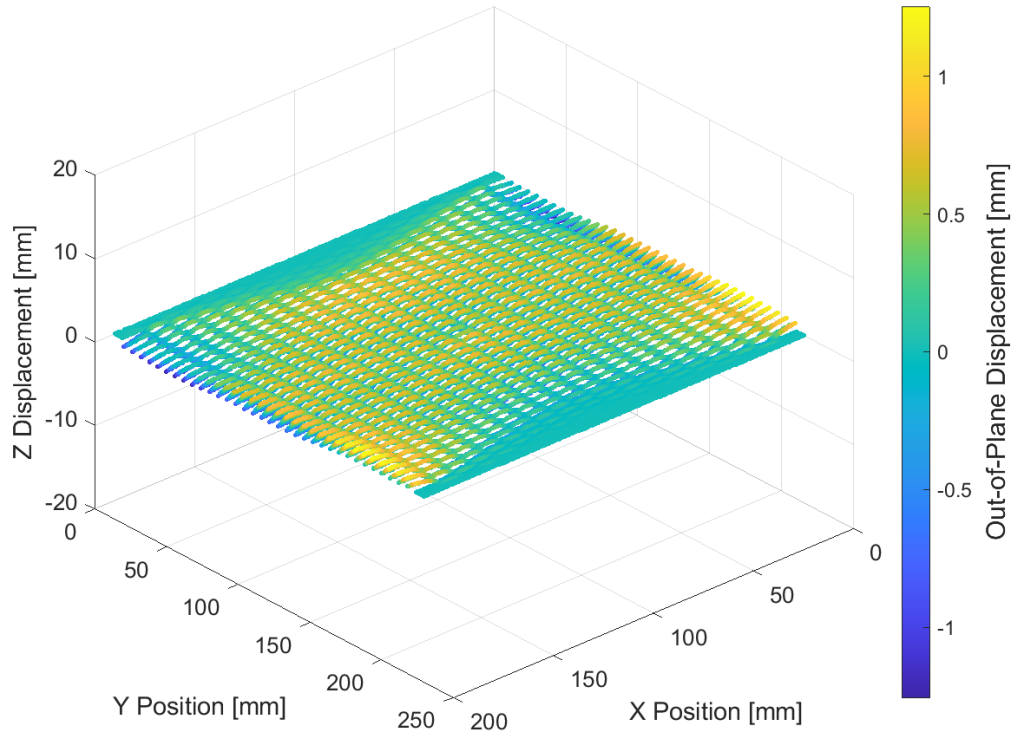


Figure 21: Anti-symmetric lattice deflection

For a symmetric deflection of the kirigami lattice, there is an alternative out-of-plane deflection along every row of cuts, but a uni-directional out-of-plane deflection along each column of cuts.

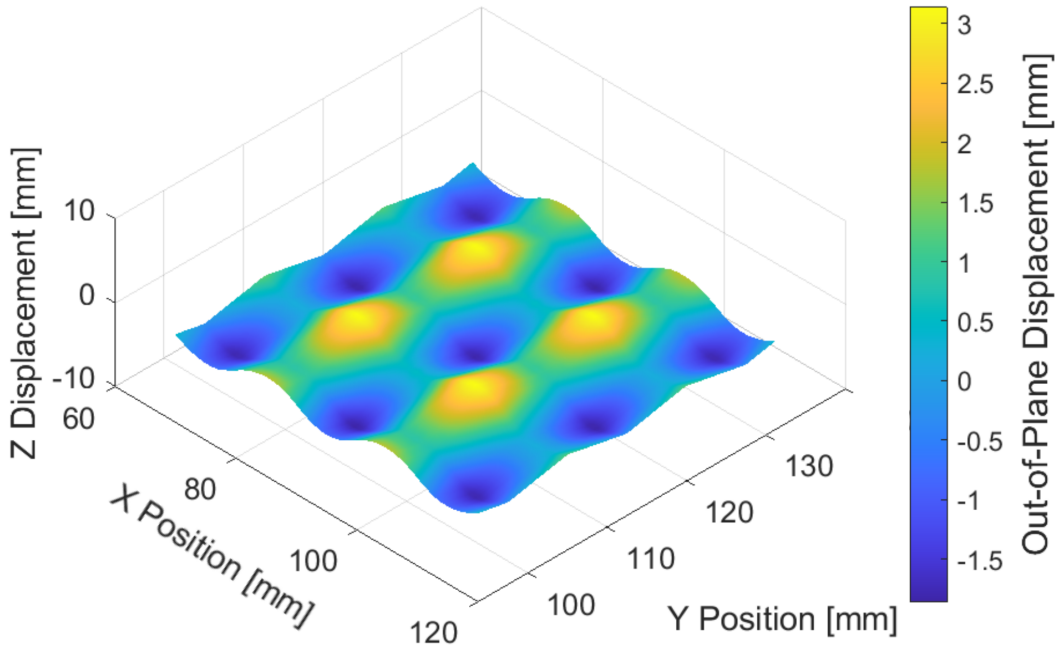


Figure 22: Close up of symmetric lattice deflection

For an anti-symmetric deflection of the kirigami lattice, the vertical area between cuts remains planar, whereas the horizontal area between cuts deforms alternatively out-of-plane above and below each cut.

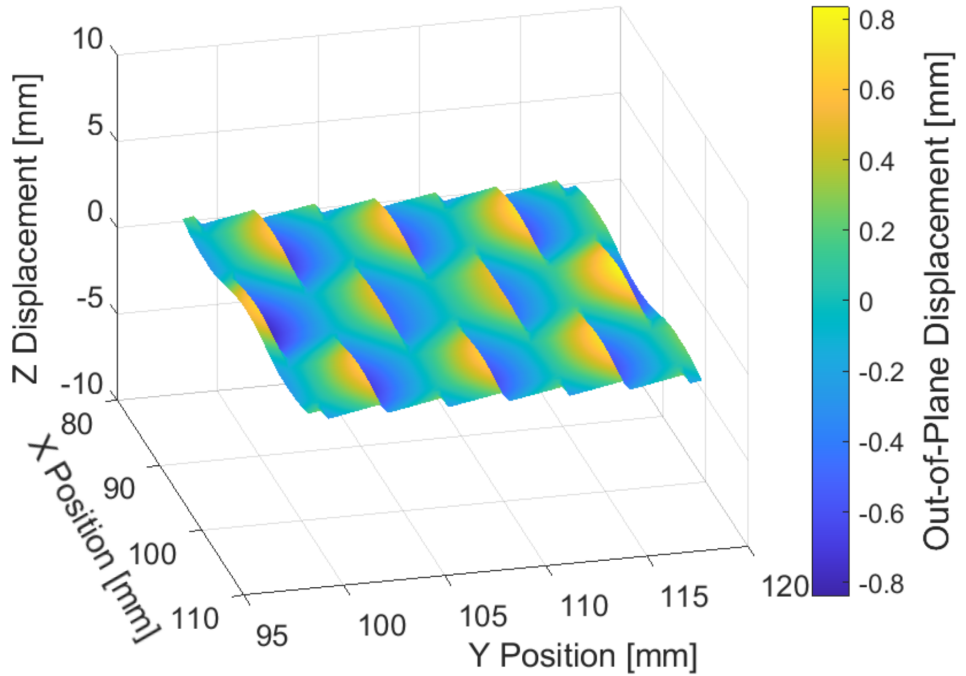


Figure 23: Close up of anti-symmetric lattice deflection

## Appendix C: DIC imaging of PRMS sheet

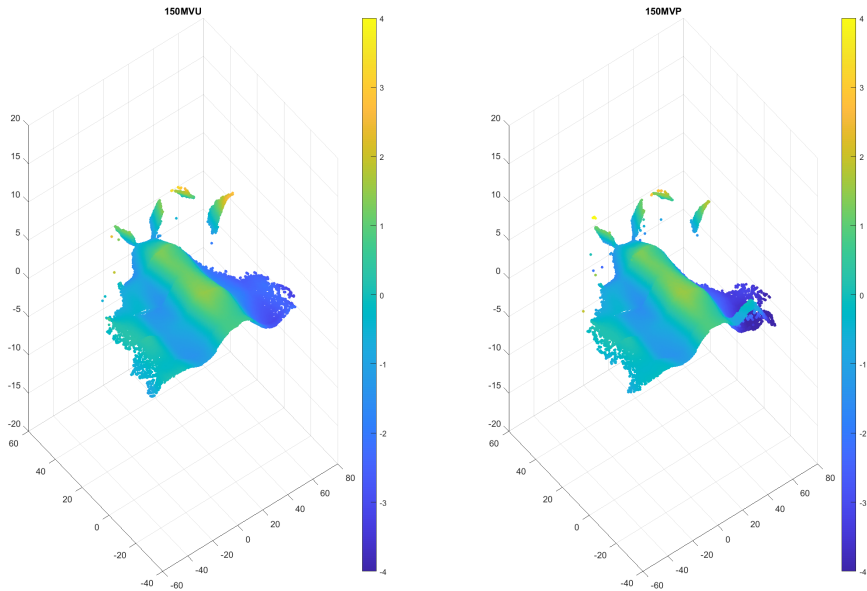


Figure 24: DIC data for deflection of PRMS sheet with vertically integrated powered and unpowered piezos